Electronic Supplementary Material (ESI) for ChemComm.

Supporting information

Spray deposited polycrystalline $MAPbBr_3$ thick films for hole-transport-material free perovskite solar cells

Qien Xu,[a†] Zhengdan Rao,[a†] Yiting Yang,[a,b] Bo Jin,[a] Xiaotian He,[a] Jiaxuan Lai,[a] Tiantian He,[a] Lin Yang,[b] Limin Zhang,[c] Yongqi Liang [a]*

[a] College of Chemistry and Chemical Engineering, Key laboratory of Advanced Catalysis of Gansu Province, Lanzhou University，Lanzhou City, Gansu Province, China 730000
[b] School of Chemistry and Chemical Engineering, Qinghai Normal University, Xi'ning City, Qinghai Province, China, 810016
[c] School of Nuclear Science and Technology, Lanzhou University, Lanzhou City, Gansu Province, China 730000
[d] National Radiation Application Center, China Institute of Atomic Energy, Beijing, China, 102413

[†] the authors contribute equally

yqliang@lzu.edu.cn

Experimental details

The chemicals of DMF (Chengdu Chron Chemical, HPLC grade, ≥99.8%), DMSO (tianjin li'anlong Bohua, analytical grade, ≥99.5%), $PbBr_2$ (Aladdin, chemical grade, 99%) were bought and used as received unless otherwise stated.

Synthesis of $MAPbBr_3$ single crystal precursors. MABr was synthesized and purified in the lab (10°C, relative humidity 40%). Concentrated HBr (Chengdu kelong chemicals, ≥40.0%) aqueous solution was added to the CH_3NH_2 dissolved in methanol (Chengdu kelong Chemicals, ≥30.0%) with a ratio of 1.05:1. The solution was kept in the ice bath to prevent side reactions in the air. With the help of rotary evaporator (70 ºC), the MABr powders were obtained by removing the solvents from the reaction mixture. The obtained MABr powder was then dissolved in methanol, then diethyl ether was added to precipitate the solid. After thorough washing with diethyl ether, white solid was obtained and dried under vacuum at 60 ºC.

Commercial $PbBr_2$ was purified by a re-crystallization process in our laboratory (9~16 °C, 20% ~50% relative humidity). $PbBr_2$ was dissolved in DMF (Tianjin li'anlong Bohua, analytical grade, ≥99.5%) which was heated at 80 ºC for 1 hour to get dissolved completely. The hot solution was filtered and ethanol (Tianjin li'anlong Bohua, analytical grade, ≥99.7%) was then added to precipitate the solid $PbBr_2$. The solid was then baked at 80ºC inside an oven to get dried before further use.

$MAPbBr_3$ single crystals were grown from the inverted crystallization process. Purified MABr and $PbBr_2$ powders were dissolved in DMF (N,N-dimethylformamide (Chengdu Chron Chemical, HPLC grade, ≥99.8%) to obtain a 1.5 M solution in MA^+ and a 1.2 M solution in Pb^{2+}. Then the solution was heated inside an oven at 120ºC to get single crystals of different sizes. Then the mother liquor was filtered when it was still hot, and small amount of DMF was added to wash off possible contaminants from the crystal surfaces. The $MAPbBr_3$ single crystals were further broken into small pieces before being dissolved as the precursor solution for spray deposition.

Fabrication of the electron transport layer of TiO_2 films on FTO. The FTO glass (TEC-15, Nippon Sheet Glass) was used as the substrate for device fabrication. The FTO substrates were cleaned via

ultrasonication in aqueous detergent solution, deionized water, acetone and iso-propanol. The cleaned substrates were then treated under O_2 plasma for 3 minutes. A thin (~30 nm) compact TiO_2 layer on top of FTO was then fabricated through spray pyrolysis. 1.8 ml Titanium (IV) isopropoxide (TITP) was dissolved in ethanol, and 1.2ml acetylaceton (AcAc) was added to make the precursor solution. Spray pyrolysis was carried out with the compressed air as the carrier gas. Each spray cycle contains a 10 seconds/ 50 seconds on/off period. The FTO substrates were kept at 450 º C during the spray pyrolysis procedure.

Spray deposition of $MAPbBr_3$ thick films on TiO_2 covered FTO. The precursor solution for spray deposition was made by dissolving $MAPbBr_3$ single crystals inside DMF. The solution (1.2M) was stirred for 1 hour before use. For the stoichiometry investigation, 2.5% excess $PbBr_2$ was added. 6% KBr was added to the precursor solution to promote the effects of K^+ during $MAPbBr_3$ film fabrication.

The spray deposition process was carried out inside a fume hood. The TiO_2 covered FTO substrates were heated on a hotplate set at 80°C. Compressed N_2 was used as the carrier gas for atomizing the liquid precursor via a nozzle. Each spray cycle lasted for 3 seconds and another 30 seconds was waited before the solvents got evaporated. The film thickness was tuned by the number of cycles for deposition. Assuming the mass density of $MAPbBr_3$ as 3.87g/cm^3, the film thickness was estimated by measuring the mass change before and after the deposition of perovskite films onto FTO substrate. Under the typical condition, $MAPbBr_3$ films of 40 um thickness could be obtained after 5 cycles of spraying and drying. Films of different thickness were deposited by repeating more spray cycles.

Fabrication of the carbon electrodes. Home-made carbon paste was prepared by dispersing synthetic graphite particles (~20 um, 1.5 g, Runze SiC company) and carbon black (0.5g, Vulcan XC-72R, Cabot) into DBE solvent (dibasic esters, 3.0 g, Dupont). The polyester polymer (1.0 g, Skybon ES-300) resin was used as the binder to make the paste with suitable viscosity for the following Dr. blading process. The quality of the carbon paste was checked by measuring the film conductivity via a 4-point probe station (JG ST2258C, Suzhou, China) after being dried at 120°C for 30 minutes. The thickness of the carbon electrodes was checked using SEM, and the resistance of carbon electrodes varied from 40 to 60 ohm/square.

Structural characterization of $MAPbBr_3$ thick films. For structure characterization, a Rigaku Ultima IV (Cu target, K_α line) diffractometer was used. The scanning rate was set at 4 º/min and the step size was 0.02º. Fluorescence spectrum (450 nm laser diode excitation, emission collected from the rear side the $MAPbBr_3$ films on FTO) and lifetime (Picoquant Fluotime 200, excitation at 455nm) were also used for the quality check of $MAPbBr_3$ thick films. For surface morphology and cross-sectional characterization, a ThermoFisher Apreo S scanning electron microscope was used.

Photovoltaic characterization of $MAPbBr_3$ thick film devices. The photovoltaic characterization of the $MAPbBr_3$ devices was carried out under ambient condition. A Oriel LCS100 solar simulator was used as the AM1.5 sunlight source, and the light intensity was calibrated with a standard Si solar cell available from Newport. The J-V curve was measured at a scanning speed of 0.1 V/sec.

The Incident Photon Conversion to electron Efficiency (IPCE) spectra of the $MAPbBr_3$ devices were collected under the DC mode via an Zolix 100 setup, and a calibrated Si photodetector as the reference sample.

Mott-Schottky analysis of thick $MAPbBr_3$ film devices was carried out in the dark via an Admiral Squidstat Plus. The voltage modulation amplitude is 10 mV, and the frequency for modulation is 3k Hz, 10k Hz and 30k Hz.

1. Morphology of a thick $MAPbBr_3$ film without KBr additive

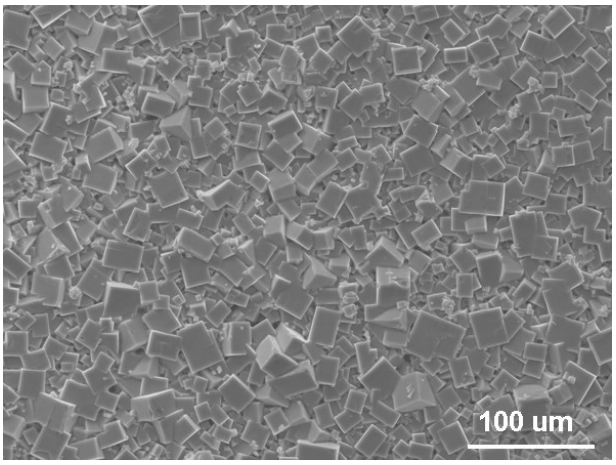

Figure S1. $MAPbBr_3$ thick films without KBr additive to the precursor solution. No dots on top of the cuboids caused by phase separation of K^+ containing phase are observed.

2. Large area thick $MAPbBr_3$ film samples

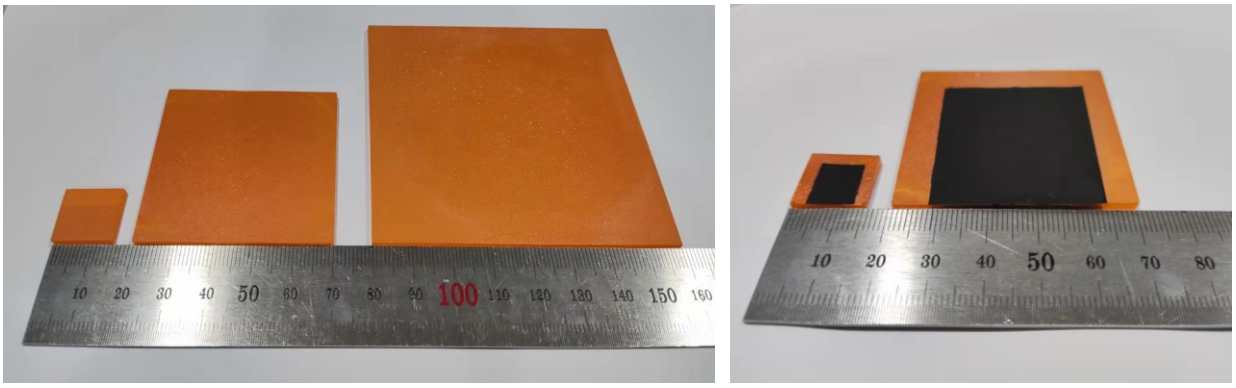

Figure S2 (left) $MAPbBr_3$ thick films of different area fabricated from the spray deposition process. The films are uniform across large areas over 8cm*8cm. (right) Thick film solar cells with carbon electrodes pasted on top.

3. Cross section of a 100um thick $MAPbBr_3$ film

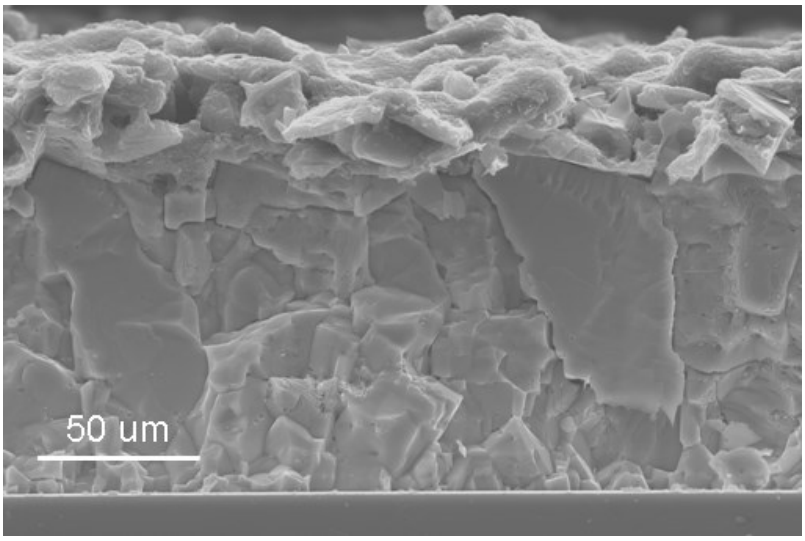

Figure S3. $MAPbBr_3$ thick films by increasing the number of cycles during spray deposition. On top of the $MAPbBr_3$ is the carbon electrode (30 um thickness) made by Dr. blading.

4. Comparison between thick film and thin film (UV-Vis)

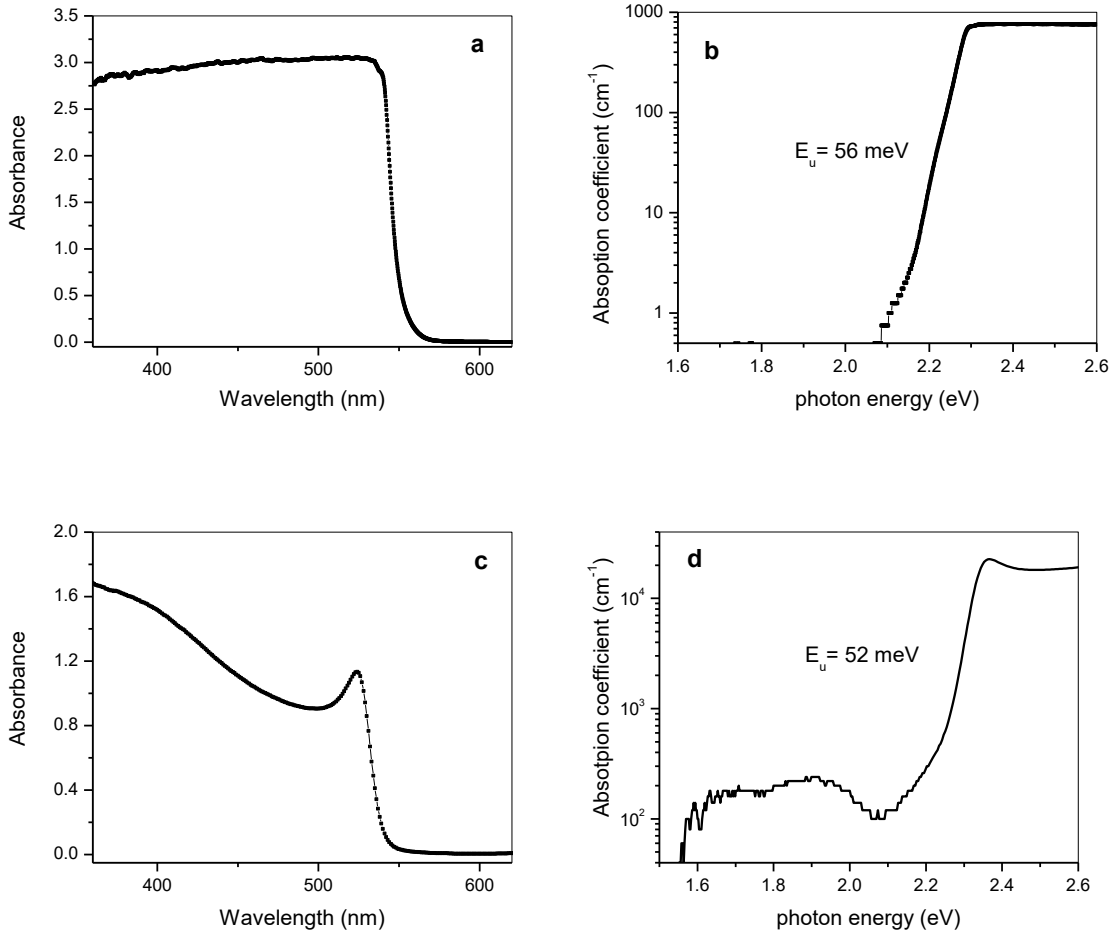

Figure S4. UV-Vis of 40 um thick $MAPbBr_3$ film (a, b) and 500 nm thin $MAPbBr_3$ film (c, d). The absorption Urbach tail energy for both thin and thick films are shown when the absorption is plotted at the logarithmic scale in **b** and **d**.

For systematic comparison, thin films of $MAPbBr_3$ were also fabricated from the previously reported anti-solvent assisted spin coating process. [1] From the UV-Vis spectrum of $MAPbBr_3$ thin films, it is obvious 500 nm thick films can absorb >95% the photons of wavelength below 550nm. The extension of the cut-off wavelength from 545 nm to 570 nm increases the theoretical short circuit current density under simulated AM1.5 sunlight from 9.32 mA/cm^2 to 11.03 mA/cm^2. The absorption Urbach tail for both thin and thick films are ~50 meV, and this suggesting that thin films and thick films are of similar quality. We also note, the Urbach energy is larger than that for $MAPbBr_3$ bulk single crystals. [2]

5. Comparison between thick film and thin film (FL spectrum)

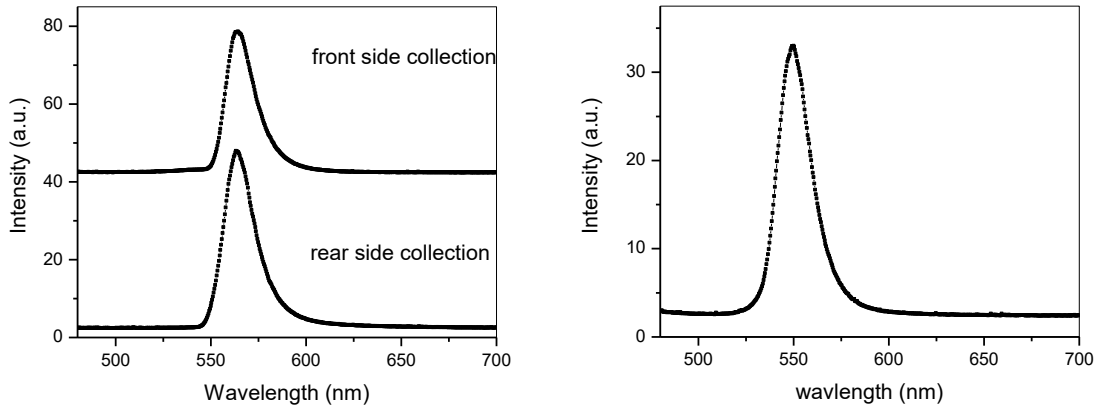

Figure S5. Fluorescence spectra for thick $MAPbBr_3$ film (left) and thin $MAPbBr_3$ film (right). For thick films, fluorescence emission spectra were both collected from front side and rear side. The peak position is 549 nm for thin films, and 564 nm for thick films, irrespective of the side for spectrum collection. The lack of red shift in the fluorescent peak collected at the rear side suggests that the re-absorption is not significant for the $MAPbBr_3$ films of 40um ~100um thickness studied here.

6. Fluorescent lifetime analysis of thick $MAPbBr_3$ film

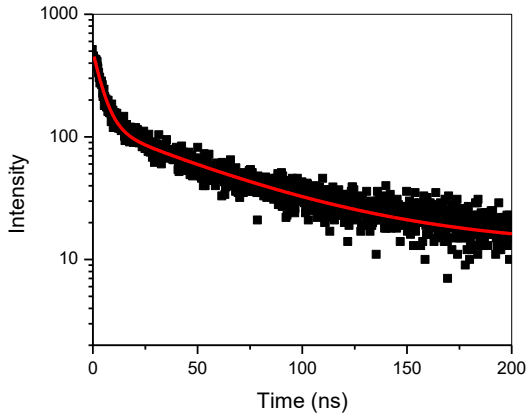

Figure S6. Fluorescence lifetime analysis of the $MAPbBr_3$ thick film. The $MAPbBr_3$ film deposited on TiO_2 covered FTO was excited via a 455 nm diode, and the emission was monitored at the wavelength of 560 nm. The fluorescence lifetime spectrum was collected via a Horiba FluoroLog3 setup. A NaonoLED was used as the light source for excitation (pulse duration is 1.4 ns, pulse intensity is 1 pJ/pulse, and the pulse repletion rate is 1M Hz). The illuminated film area is 0.038 cm^2.

The average fluorescence lifetime on the scale of 20 ns here falls in the lifetime range frequently observed for $MAPbBr_3$ nanocrystals (20 ~ 200 ns)[3;4], films (5 ~ 40 ns [5] or 7 ~ 200 ns[6]) and single crystals (10 ns ~500ns). [7;8]

7. Stability of $MAPbBr_3$ thick film solar cells

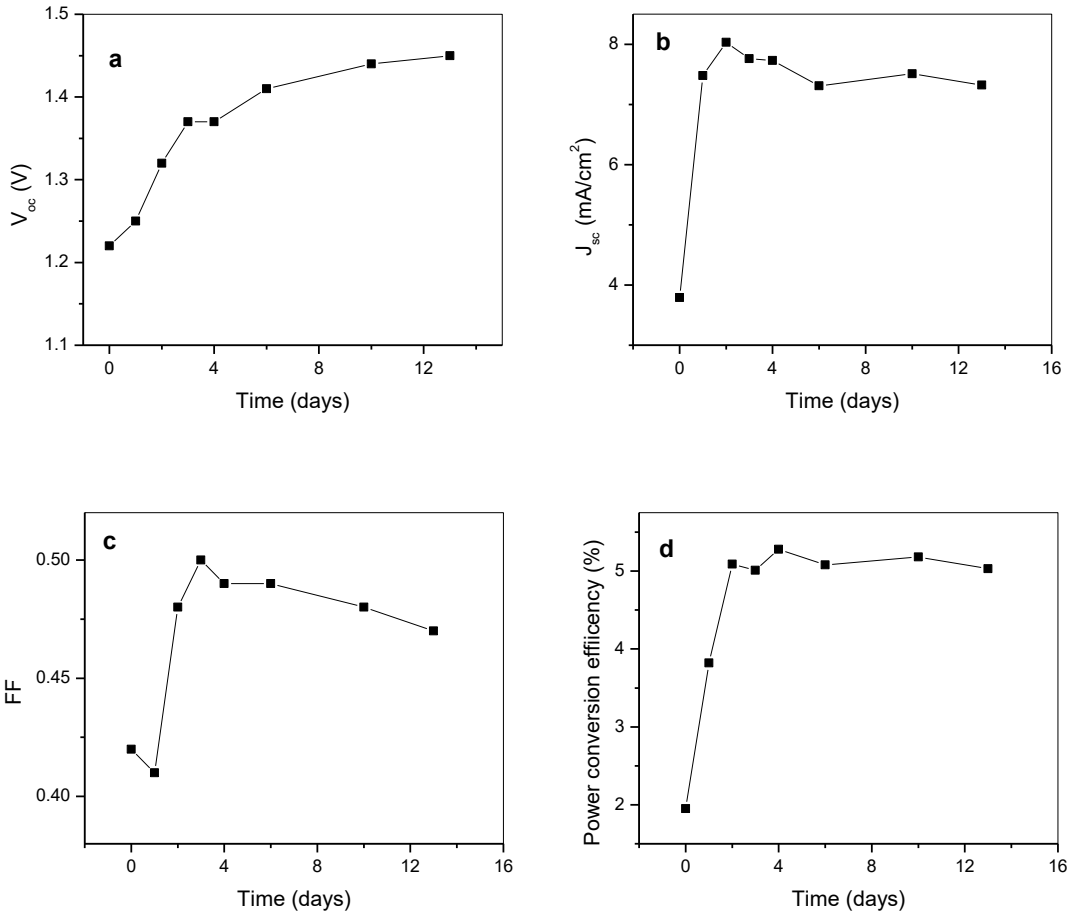

Figure S7. Shelf stability of the $MAPbBr_3$ thick film (40um thickness) solar cell.

8. Effects of K^+ on the photovoltaic performance evolution for $MAPbBr_3$ thick film solar cells

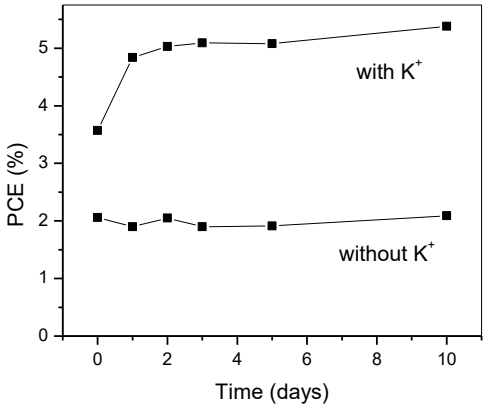

Figure S8. Comparison of the photovoltaic performance evolution of the $MAPbBr_3$ solar cells during storage in the air. For the solar cell which top trace represents, K^+ was added to the pre-synthesized $MAPbBr_3$ crystal precursor solution. For the solar cell which bottom trace represents, no K^+ was added.

The PCE of the solar cell is almost constant during the 10 days storage time when no K+ was added, which forms contrast to that for the solar cell when K+ was added to the precursor solution.

9. Hysteresis inside the J-V curve for thick $MAPbBr_3$ film solar cells

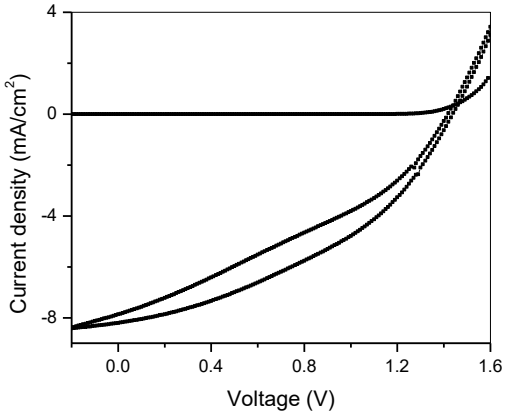

Figure S9. Hysteresis in J-V for the $MAPbBr_3$ thick film solar cell. Both the J-V curve in the dark and J-V curve under simulated AM1.5 sunlight are shown. The main difference comes from the low fill factor when scanning in the direction from -0.2V (reverse bias) to +1.6V (forward bias).

Due to the hysteresis inside J-V curve, the photovoltaic performance data reported in this article were always measured in the scanning direction from +1.6 V to -0.2 V, unless otherwise stated.

10. Mott-Schottky analysis of *thin* $MAPbBr_3$ film

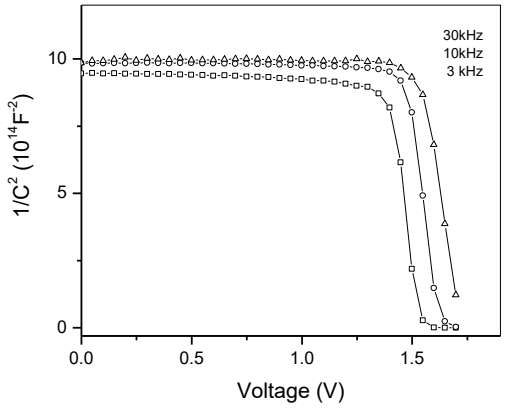

Figure S10. Mott-Schottky plots for a thin $MAPbBr_3$ film device. Frequency dispersion exists in Mott-Schottky plots for thin $MAPbBr_3$ films. The acceptor density inside thin $MApbBr_3$ thin films is on the order of $10^{15}cm^{-3}$, which is almost 10^4 times higher than that for thick $MAPbBr_3$ films. The V_{oc} measured under simulated AM1.5 sunlight for the same device falls inside the range of the built-in voltage derived from Mott-Schottky plots.

11. Raman characterization of the $MAPbBr_3$ thick films

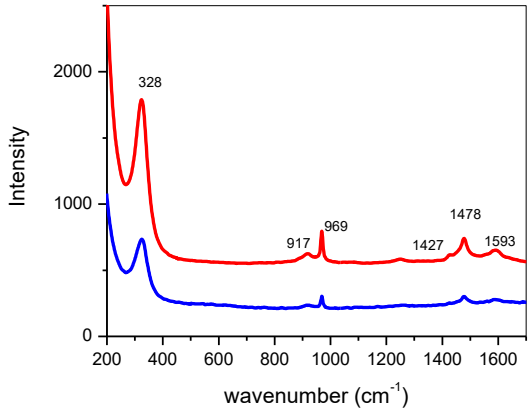

Figure S11. Room-temperature Raman spectra of the pre-synthesized $MAPbBr_3$ single crystals grown via the inverted temperature crystallization (upper trace) and the thick $MAPbBr_3$ films grown from spray deposition (lower trace). All the Raman peaks can be assigned to $MAPbBr_3$ and marked by the corresponding wavenumber. The Raman spectra were collected on a micro-Raman setup (Horbiba LabRam HR Evolution), and the excitation wavelength was 633 nm.

The fingerprint vibrational peak from DMA at 888 cm^{-1} in the Raman spectrum[9] was not found in both the single crystal $MAPbBr_3$ precursors and the spray-deposited $MAPbBr_3$ films. This proves that there is no DMA incorporation inside $MAPbBr_3$ under the conditions we used here. The absence of DMA might be due to the negligible extent of DMF decomposition under the synthesis conditions.

12. Statistical data on highly efficient solar cells of $MAPbBr_3$ thick films

	η(%)	V_{oc} (V)	J_{sc} (mA/cm^2)	FF
1	5.17	1.43	8.35	0.43
2	5.27	1.48	8.43	0.42
3	5.52	1.43	8.55	0.45
4	5.32	1.43	7.97	0.47
5	5.03	1.58	7.14	0.44
6	5.47	1.54	7.31	0.49
7	5.15	1.41	7.96	0.46
8	5.07	1.41	7.31	0.49
9	5.17	1.44	7.51	0.48
10	5.17	1.37	7.72	0.49
11	5.51	1.54	7.31	0.49
12	5.89	1.64	7.81	0.46
13	5.73	1.60	8.20	0.44
14	5.65	1.60	8.00	0.44
15	5.81	1.60	7.72	0.47

Table S1. Device performance of a serie of solar cells with power conversion efficiency >5%. We specifically note that the Fill Factor for thick solar cells is low (<0.50), which forms contrast to the reported $MAPbBr_3$ thin film solar cells (FF >0.65).

13. Using pre-synthesized $MAPbBr_3$ crystals as the precursor is superior compared to using $PbBr_2$ and MABr mixture as the precursor for $MAPbBr_3$ thick film solar cells

	V_{oc} (V)	J_{sc} (mA/cm^2)	FF	η (%)
pre-synthesized $MAPbBr_3$ crystal precursor	1.460 ± 0.032	7.69 ± 0.36	0.41 ± 0.01	4.62 ± 0.34
$PbBr_2$ and MABr mixture precursor	1.096 ± 0.024	2.58 ± 0.27	0.60 ± 0.05	1.70 ± 0.15

Table S2. Comparison between the photovoltaic performance for $MAPbBr_3$ thick film solar cells, which are made from either pre-synthesized single crystal of $MAPbBr_3$ precursor and $PbBr_2$/MABr mixture precursor (8 devices for each batch).

As shown in **Table S2**, The $MAPbBr_3$ thick films made from the pre-synthesized $MAPbBr_3$ crystal precursor systematically outperform the $MAPbBr_3$ thick films made from the $PbBr_2$ and MABr mixture precursor. Similar results have been reported for perovskite solar cells of in the literature.[10;11]

Reference List

1. Y. Liang, Y. Wang, C. Mu, S. Wang, X. Wang, D. Xu, and L. Sun, *Advanced Energy Materials*, 2018**, 8**, 1701159.
2. S. De Wolf, J. Holovsky, S. J. Moon, P. L+¦per, B. Niesen, M. Ledinsky, F. J. Haug, J. H. Yum, and C. Ballif, *The Journal of Physical Chemistry Letters*, 2014**, 5**, 1035.
3. S. Gonzalez-Carrero, L. Franc+¬s-Soriano, M. a. Gonz+ílez-B+¬jar, S. d. Agouram, R. E. Galian, and J. P+¬rez-Prieto, *Small*, 2016**, 12**, 5245.
4. T. Cai, F. Li, Y. Jiang, X. Liu, X. Xia, X. Wang, J. Peng, L. Wang, and W. A. Daoud, *Nanoscale*, 2019**, 11**, 1319.

5. F. Ye, H. Wu, M. Qin, S. Yang, G. Niu, X. Lu, J. Wang, D. B. Mitzi, and W. C. H. Choy, *ACS Applied Materials & Interfaces*, 2020**, 12**, 24498.

6. M. I. Saidaminov, V. Adinolfi, R. Comin, A. L. Abdelhady, W. Peng, I. Dursun, M. Yuan, S. Hoogland, E. H. Sargent, and O. M. Bakr, *Nature Communications*, 2015**, 6**, 8724.

7. H. Wei, Y. Fang, P. Mulligan, W. Chuirazzi, H. H. Fang, C. Wang, B. R. Ecker, Y. Gao, M. A. Loi, L. Cao, and J. Huang, *Nature Photonics*, 2016**, 10**, 333.

8. B. Wenger, P. K. Nayak, X. Wen, S. V. Kesava, N. K. Noel, and H. J. Snaith, *Nature Communications*, 2017**, 8**, 590.

9. M. Ptak, A. G-àgor, A. Sieradzki, B. Bondzior, P. Dere+ä, A. Ciupa, M. Trzebiatowska, and M. M-àczka, *Physical Chemistry Chemical Physics*, 2017**, 19**, 12156.

10. Y. Qin, H. Zhong, J. J. Intemann, S. Leng, M. Cui, C. Qin, M. Xiong, F. Liu, A. K. Y. Jen, and K. Yao, *Advanced Energy Materials*, 2020**, 10**, 1904050.

11. G. S. Shin, Y. Zhang, and N. G. Park, *ACS Applied Materials & Interfaces*, 2020**, 12**, 15167.